CDF Note 10105 v1.1

Search for Higgs Bosons Produced in Association with b-Quarks

The CDF Collaboration

URL http://www-cdf.fnal.gov

(Dated: June 13, 2010)

We present a search for neutral Higgs bosons decaying into $b\bar{b}$, produced in association with b quarks in $p\bar{p}$ collisions. This process could be observable in supersymmetric models with high values of $\tan\beta$. We search for an enhancment in the mass of the two lead jets m_{12} in triply b-tagged events, using a data sample corresponding to 2.2 fb^{-1} of integrated luminosity collected with the CDF II detector at the Fermilab Tevatron collider. The dijet mass spectrum of the heavy flavor multi-jet background is derived from double-tagged data in a manner that accounts for tagging biases and kinematic differences introduced by the addition of the third tag. The levels of background and possible signal are determined by a two-dimensional fit of the data, using m_{12} and an additional variable x_{tags} which is sensitive to the flavor composition of the three tagged jets. We set mass-dependent limits on $\sigma(p\bar{p} \to Hb) \times BR(H \to b\bar{b})$ which are applicable for a narrow Higgs or other scalar particle produced in association with b quarks. We also interpret the results as limits on $\tan\beta$ in MSSM models including the effects of the Higgs width.

Preliminary Results for Winter 2010 Conferences

FIG. 1: MSSM Higgs cross sections for various production modes at $\tan\beta = 40$ in the m_h^{max} scenario, from the TeV4LHC Working Group [2].

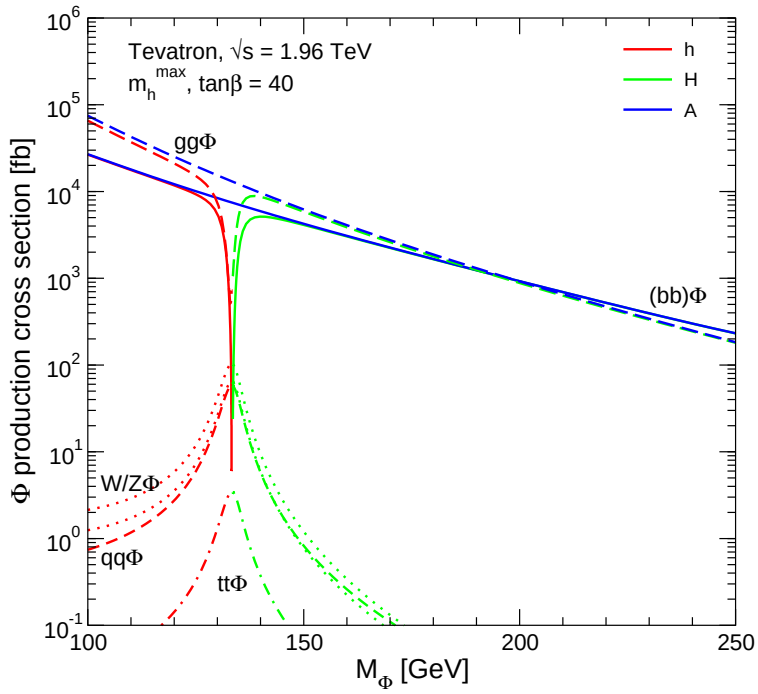

I. INTRODUCTION

The production rate of light Higgs bosons in association with b-quarks can be significantly enhanced in supersymmetric extensions of the standard model. This occurs for large values of $\tan\beta$, the ratio of the Higgs coupling to down-type versus up-type quarks. Figure 1 shows the cross section expected for $\tan\beta = 40$ in the m_h^{max} benchmark scenario [1], from the TeV4LHC Working Group [2]. The cross section for $(bb)\Phi$ is in the 10 pb range, which could potentially be observable at the Tevatron. Also interesting is that at large $\tan\beta$ the pseudoscalar A becomes degenerate with either the light (h) or heavy (H) scalar, giving an effective factor of two enhancement to the cross section.

The cross sections shown in Figure 1 are for inclusive production [3], however only the case where at least one of the b's accompanying the Higgs is at high p_T is relevant to these results, since we will require that it be b-tagged. As shown in Figure 2, cross section calculations are available for this case as well [4, 5, 6, 7], allowing for the interpretation of the results of the search described in this note.

Results for the Higgs+1b process in the case of Higgs decays to $b\bar{b}$ have been obtained by DØ [8, 9, 10], and for Higgs production in the $\tau\tau$ decay mode by CDF [11, 12] and DØ [13, 14, 15].

In this analysis we search for Higgs decays into $b\bar{b}$, accompanied by an additional high-p_T b, giving an event signature of at least three b-jets. We study the dijet mass

FIG. 2: MSSM Higgs cross sections at $\tan\beta = 40$ as a function of the number of high-p_T b quarks accompanying the Higgs (taken from Ref. [5]).

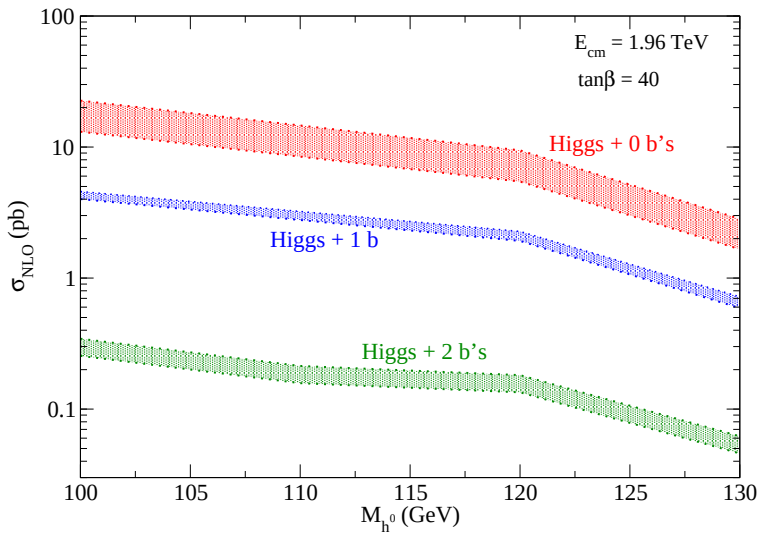

FIG. 3: The tag mass m^{tag} for different jet flavors.

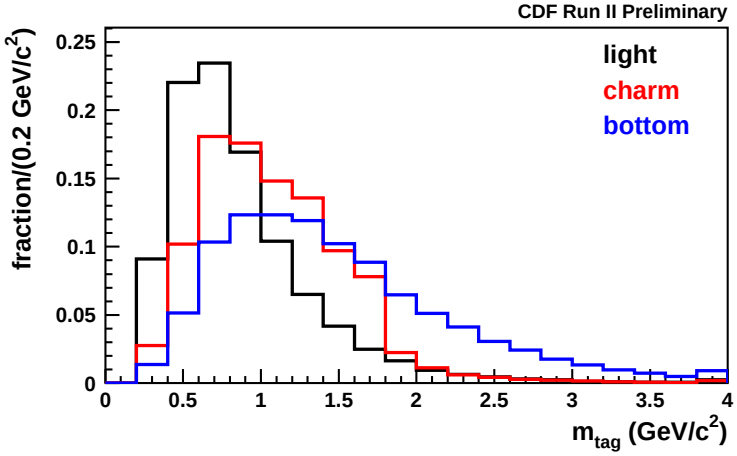

spectrum of the two leading jets in three-jet events with all three jets identified as b-jet candidates using a displaced vertex algorithm [16]. We use the dijet mass of the two leading jets in the events m_{12} to separate Higgs signal from background events. We also define a quantity $x_{tags}(m_1^{tag} + m_2^{tag}, m_3^{tag})$, where m_i^{tag} is the mass of the tracks forming the displaced vertex in jet 1, 2, or 3. The m^{tag} are sensitive to the flavor of the jet as shown in Figure 3.

FIG. 4: Illustration of the x_{tags} definition.

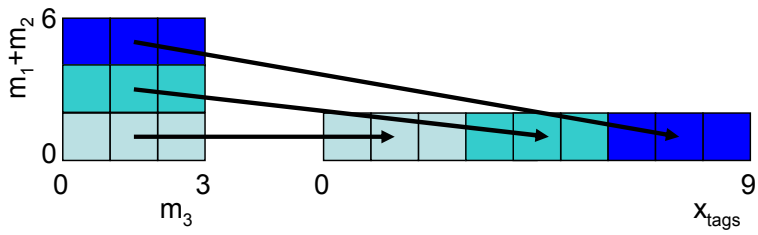

The x_{tags} variable is defined as

$$x_{tags} = \begin{cases} \max(m_3^{tag}, 2.99) & : \quad m_1^{tag} + m_2^{tag} < 2 \\ \max(m_3^{tag}, 2.99) + 3 & : \quad 2 \leq m_1^{tag} + m_2^{tag} < 4 \\ \max(m_3^{tag}, 2.99) + 6 & : \quad m_1^{tag} + m_2^{tag} \geq 4 \end{cases} \tag{1}$$

where $\max(a, b)$ returns the maximum of a and b, and all quantities are in units of GeV/c^2. The net effect is to unstack a two-dimensional histogram of $m_1^{tag} + m_2^{tag}$ versus m_3^{tag} into the one-dimensional variable x_{tags}, as illustrated in Figure 4.

II. DATA SAMPLE & EVENT SELECTION

This analysis is based on an integrated luminosity of 2.2 fb^{-1} collected with the CDF II detector [17] between February 2002 and July 2008. The data are collected on a trigger requiring two central energy clusters with $E_T > 15$ GeV, along with two tracks with $p_T > 2$ GeV/c and impact parameter $|d_0| > 100$ μm reconstructed using the Level2 silicon vertex tracker system.

The offline selection requires three jets with $E_T > 20$ GeV and detector rapidity $|\eta| < 2$. The jets are reconstructed using a cone algorithm with radius $\delta R = \sqrt{\delta\phi^2 + \delta\eta^2} < 0.7$, and are corrected for calorimeter response and multiple interactions so that the energy scale mirrors the total p_T of all particles within the jet cone. The two leading jets in the event must match to the 15 GeV energy clusters and displaced tracks in the Level2 trigger selection. The track matching allows for the case where both tracks are matched to a single one of the two lead jets, or where each of the two jets has one of the tracks matched. All three of the jets must be tagged as b-jets using the SECVTX algorithm [16], which searches for displaced b-decay vertices using the tracks within the jet cone. We also select an auxiliary sample with no SECVTX tag requirement on the third jet which is used for constructing background estimates.

To compute the efficiency of this selection, the cross section being measured must be precisely defined. We use the MCFM program to calculate the cross section for $bg \to H + b_{jet}$ which corresponds to the three-b-jet event selection. The notation b_{jet} refers to the clustering of final-state partons performed by MCFM. If there is a gluon in the final state along with the outgoing b quark (MCFM does not decay the

FIG. 5: SM cross section for $bg \to H + b_{jet}$ calculated with MCFM.

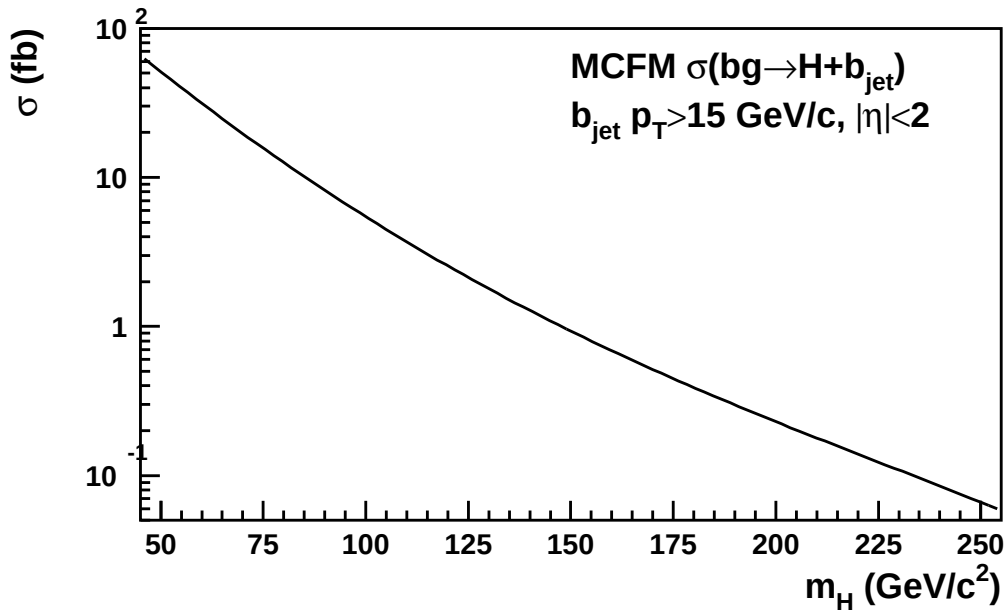

Higgs) and they are within $\delta R < 0.4$ of each other, MCFM will combine them into a "jet", otherwise the b quark alone serves as the jet. This b-jet is the object upon which the kinematic cuts can be applied.

We calculate the cross section for $H + b_{jet}$ in the SM, requiring $p_T > 15$ GeV/c and $|\eta| < 2$ for the b_{jet} to match the b-tagging acceptance of the SECVTX algorithm. We used CTEQ6.5M [18] parton distribution functions and set the renormalization and factorization scales to $\mu_R = \mu_F = (2m_b + m_H)/4$ as suggested in Refs. [7, 19]. The cross section obtained as a function of m_H is shown in Figure 5.

The efficiency of this selection on bH events where the Higgs decays into a $b\bar{b}$ pair is determined from simulated data generated using the PYTHIA [20] Monte Carlo program. The subprocess $gg \to b\bar{b}H$ (`MSUB=121`) is used, with a cut of $p_T > 15$ GeV/c applied to the "beam-side" b quark to reduce generation and simulation time. To more directly match the MCFM cross section calculation at least one associated parton-level b-jet (not b quark) with $p_T > 15$ GeV/c and $|\eta| < 2$ is also required. These b-jets are constructed by running the cone clustering algorithm ($\delta R = 0.4$) on all partons (quarks and gluons) in the event record, after removing those from the Higgs decay, and then choosing only those with a b quark within the jet cone. This requirement rejects events with a hard final state radiation off the b-quark that passed the PYTHIA generation p_T cut. The events are weighted with CTEQ6.5M PDFs, and a small correction is applied to broaden the b_{jet} η distribution to match the MCFM prediction.

The performance of the SECVTX algorithm in the Monte Carlo samples is calibrated to match the data using a procedure similar to that described in Ref. [16],

FIG. 6: Selection efficiency for bH events as a function of the Higgs mass m_H.

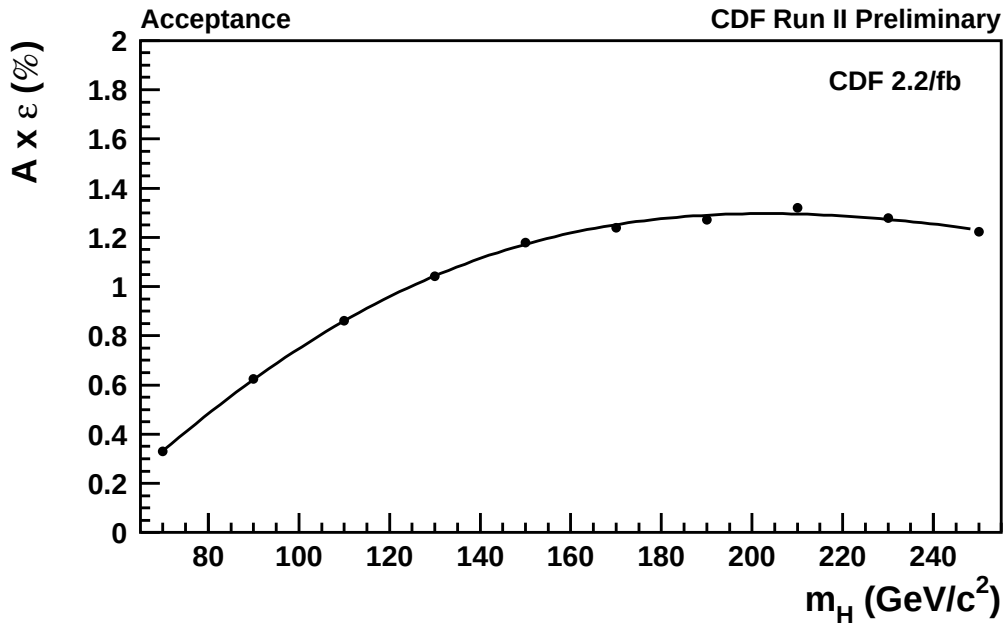

modified to include the effects of the Level2 silicon tracking requirements. The efficiency of the trigger energy cluster matching is also corrected to match the data as a function of the jet E_T. The event selection efficiencies vary from 0.4% to 1.3% as a function of the mass of the Higgs boson and are shown in Figure 6.

The mass of the two leading jets in the event m_{12}, which is used to separate signal from background in our fits, and the SECVTX tag mass combination x_{tags} are shown in Figure 7 for five values of the Higgs mass. For intermediate mass points we derive distributions by histogram interpolation and estimate the selection efficiency using the parametrization shown in Figure 6.

III. BACKGROUNDS

The three-tag sample background is essentially all QCD heavy flavor multijet production. Other processes such as $t\bar{t}$ production and $Z \to b\bar{b}$ + jets were also considered but found to contribute at a negligible level. Using simulated samples of generic QCD multijet production produced with PYTHIA [20] to develop and test our methods, we find that virtually all of the QCD background in our selected triple-tag sample consists of events with at least two real b-tags, with the additional tag being any of a mistagged light jet, a c-tag, or another b-tag. The double-tagged three jet events are found to be predominantly two real b-tags, which makes them a natural starting point for constructing background estimates.

We describe the flavor structure of the jets in the event in the form XXY, where XX is the flavor of the two leading jets (i.e. bq would mean a b-jet (b) and a mistagged

FIG. 7: Distributions of m_{12} (top) and x_{tags} (bottom) for the Higgs signal samples, binned in the indicated increments. The lines simply connect the bin centers and do not represent parametrizations. All are normalized to unit area.

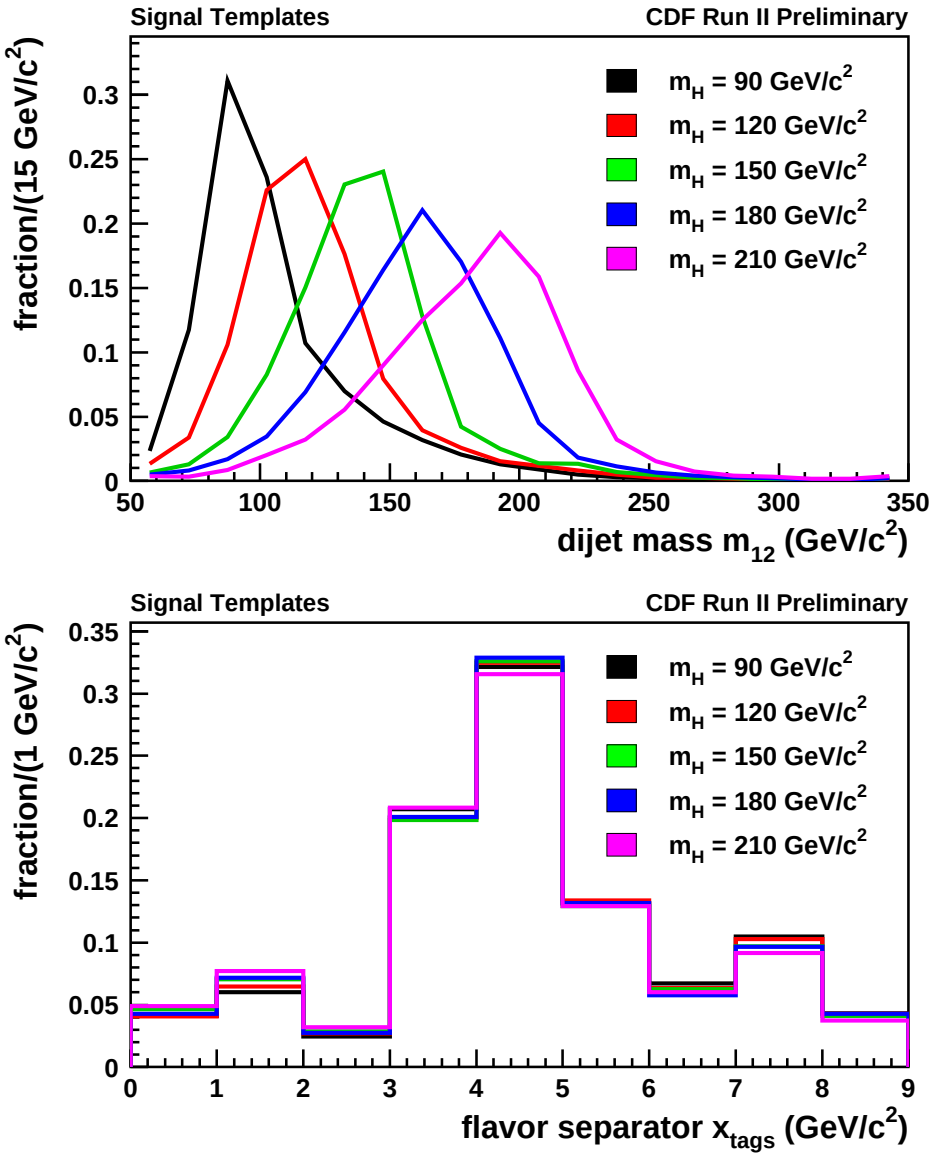

light quark (or gluon) jet (q)), while Y is the flavor of the third-leading jet. We make no distinction between the leading and second-leading jets, so that in a *bcb* event the charm tag could be either of the two leading jets. Under this convention we identify five types of event with at least two real b-tags. Three involve b-tags on both of the leading jets: *bbb*, *bbc*, and *bbq*. The other two, *bcb* and *bqb*, have the non-b-tag in one of the two leading jets. The templates we use in our fits for each of these components are shown in Figure 8. In the plot we combine *bbc* and *bbq* into

FIG. 8: Distributions of m_{12} (top) and x_{tags} (bottom) for the background fit templates, binned in the indicated increments. The lines simply connect the bin centers and do not represent parametrizations. All are normalized to unit area.

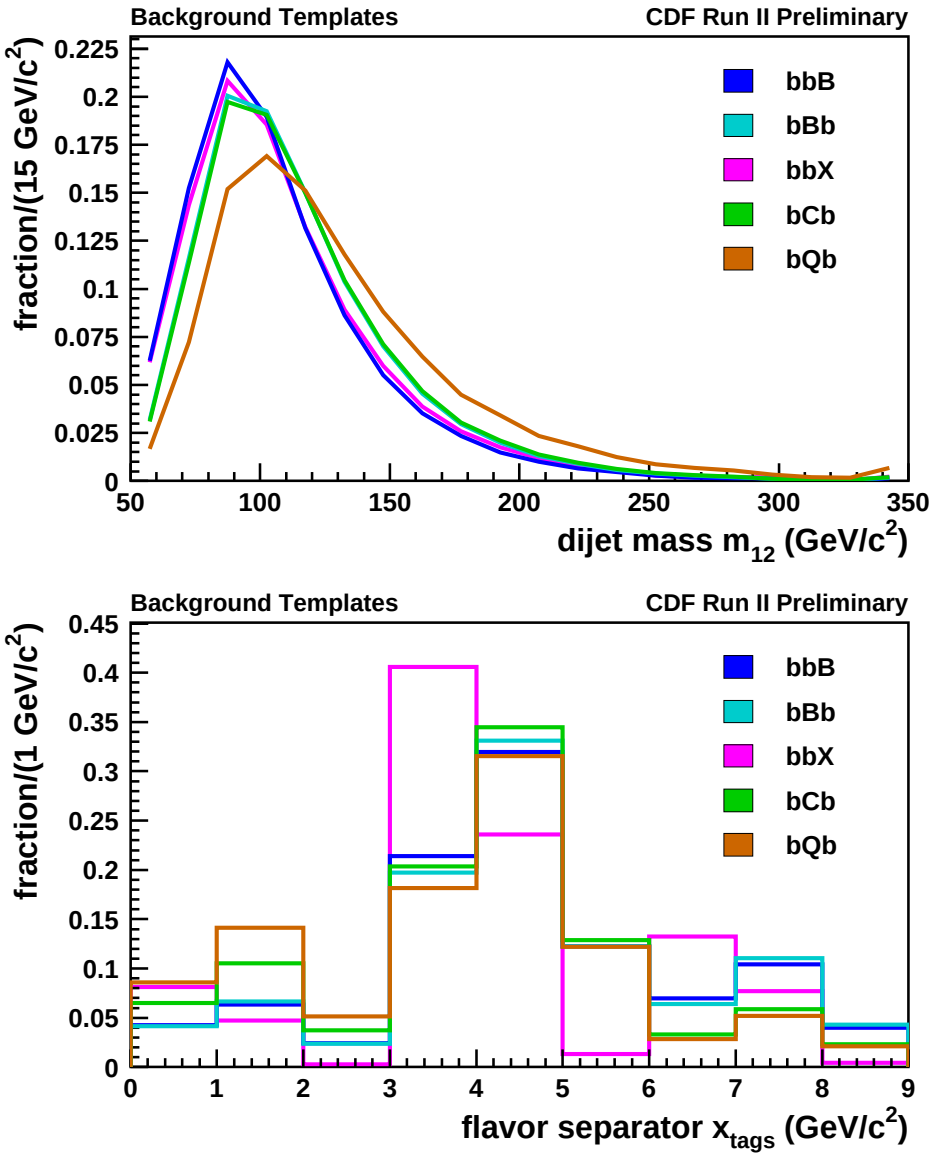

a single 'bbx' shape because they are very similar. Descriptions of our methods for producing these templates follow.

A. General procedure

As noted above, the events with the two leading jets tagged and a third jet are found to largely consist of two real b-tags. This makes them an excellent starting point for constructing estimates of the bbb, bbc, and bbq backgrounds. In order to turn these double-tagged events into estimates of the triple-tagged sample we must simulate the effect of tagging the third jet. This is done using parametrizations of the SECVTX tag efficiency derived from large samples of simulated b, c, and light-flavor jets. The tag efficiencies are parametrized as a function of the jet E_T and the number of tracks in the jet passing the SECVTX quality cuts (but with no impact parameter requirement). The jet for which the tagging has been simulated is denoted by the capital letter in Figure 8, so that for example bCb indicates that the two observed tags are both b tags, one in the third jet and one in the two lead, and the event has been weighted by the probability of the other of the two lead jets to be tagged if it came from a charm quark. The parametrizations also give a probability density for the SECVTX tag mass for a jet, defined as the mass of the tracks assigned to the displaced vertex. These tag masses are combined to produce a second discriminating variable alongside m_{12} as described below.

In addition to weighting the events to simulate the third jet tagging, we subtract the component of the double-tagged sample that is not two real b-tags. This is done using events which have two displaced vertices, but where one or both of them are on the opposite side of the primary vertex from the jet direction (negative tags) which are predominately fake tags from light-flavor jets. We weight these events in the same way and then compute

$$N_{b\bar{b}} = N_{++} - \lambda N_{+-} + \lambda^2 N_{--} \tag{2}$$

where N_{++} is the weighted count of observed double-tags in a particular bin of m_{12} and x_{tags}, N_{+-} is the corresponding quantity for events with one of the tags negative, and N_{--} is for both tags negative. The parameter $\lambda = 1.4 \pm 0.2$ reflects the difference between the negative tag rate and the light-flavor fake tag rate, due to the latter including tags from K_S/Λ and interactions with the detector material which will not be present in the negative tags. The effect of this correction on the bCb background shape is shown in Figure 9. This correction is applied to all of the background templates described below.

B. The *bbC* and *bbQ* backgrounds

Starting from the corrected double-tagged sample which we call bbj, where j means an untagged third jet, we weight the events by the probability to tag the third jet if it were a c-jet or a light jet to produce estimates for the shapes of the bbC and bbQ background components, respectively. We float these components in an unconstrained fit to the data, so it is not necessary to know how many of the third jets are actually of each flavor, only to get the shapes of the m_{12} and x_{tags} distributions correct. Because the resulting shapes are too similar to fit indepen-

FIG. 9: Distributions of m_{12} (top) and x_{tags} (bottom) used to construct the corrected bCb background template.

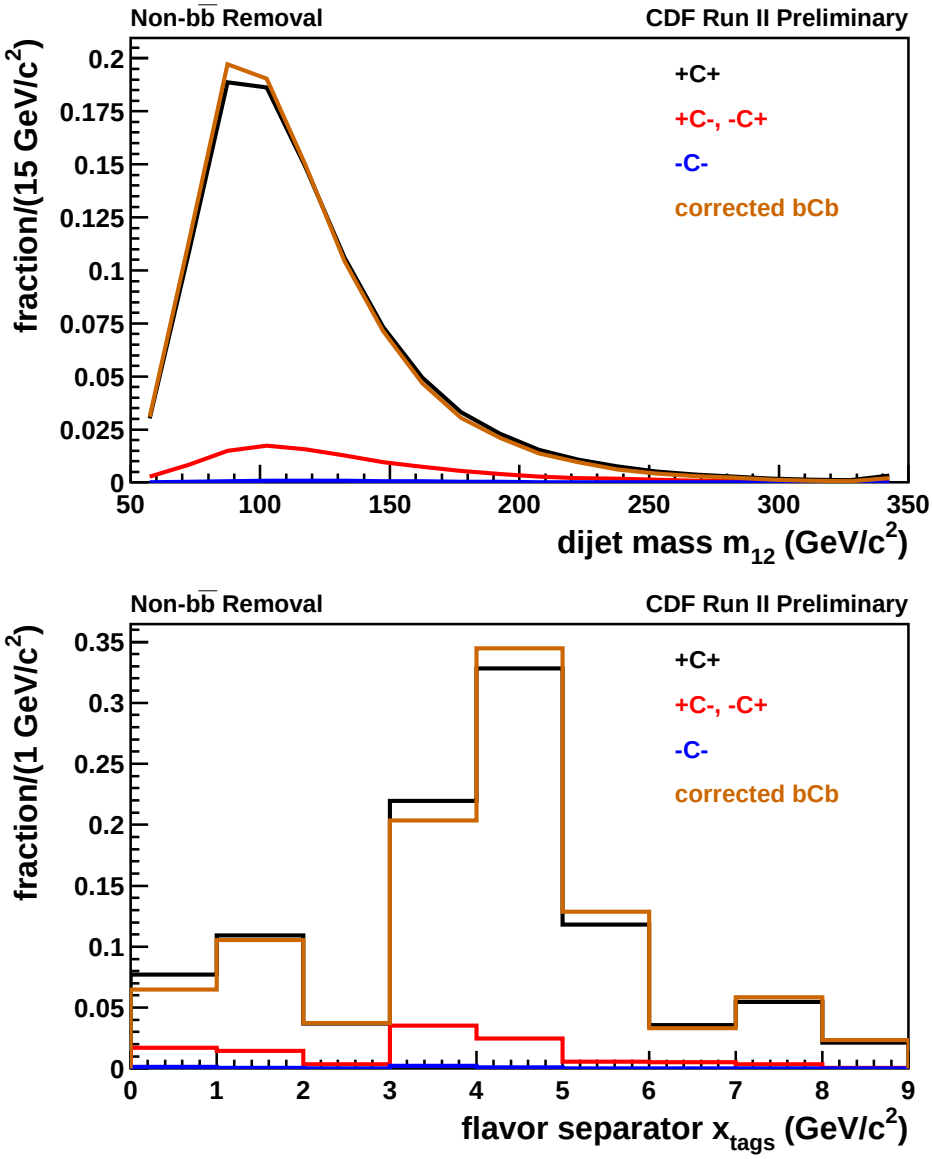

dently, we combined them into the single 'bbX' template shown in Figure 8. The small difference between them is treated as a systematic uncertainty.

C. The bbB and bBb backgrounds

The third-jet weighting procedure works very well for bbC and bbQ backgrounds, because the b-quark production physics is the same as in the bbj events used as the

starting point. For the three-b-tag background this is not the case. In bbj events there is a contribution from events with a gluon splitting into a $b\bar{b}$ pair, with those two b-jets representing the two leading jets. We find that in these events the two lead jets are less back-to-back than in events where the $b\bar{b}$ are produced directly in the hard scattering process, and therefore have a softer m_{12} distribution. Therefore, a bbB template derived from bbj events is not a good estimate for the triple-b-tagged part of the background.

In bbb events, PYTHIA indicates that although there is still a sizeable contribution from $b\bar{b}$ pairs produced through gluon splitting, there must be two such splittings in the event and there is no reason why the two lead jets have to come from the same gluon. In fact we find no significant differences in the m_{12} spectra for bbb events between the different heavy flavor production mechanisms because of this ability to almost always choose a back-to-back pair.

Besides bbB, there is a second way to produced a triple-b-tagged background template from the data. This is to start with double-tagged events where one of the tags is in the third jet and to weight the untagged jet (of the two lead jets) by the b-tag efficiency. This is the bBb template shown in Figure 8. In contrast to bbB which is too soft in m_{12}, the PYTHIA generator-level studies indicate that the m_{12} spectrum in these $b\bar{b}$ events is harder than in the triple-b-tagged ones. This relationship persists across all heavy-flavor production mechanisms, so we can safely conclude that the triple-b-tagged distribution can be derived from a weighted average of the two templates bbB and bBb. We include both in the fit and let the data determine the proper weighting. Because they are both three b-tags the two templates are very similar in x_{tags}.

D. The *bCb* and *bQb* backgrounds

These backgrounds are constructed in essentially the same way as bbC and bbQ. The only difference is that we start from a double-tagged sample where one of the tags is in the third jet rather than the two leading. From there we weight the untagged jet in the two lead jets with either the charm-tag efficiency or the light-flavor jet mistag probability.

E. Backgrounds summary

The full set of background fit templates is shown in Figure 8. The backgrounds with two heavy flavor tags in the leading jet pair have similar m_{12} distributions, while bQb displays a harder spectrum due to the mistag bias. The backgrounds separate into three groups in the x_{tags} view, with bbC and bbQ exhibiting the softest spectra, bCb and bQb in the middle, and bbB and bBb (and the Higgs signal) the hardest spectrum.

TABLE I: Summary of systematic uncertainties.

source	variation	applies to	type
luminosity	$\pm 6\%$	signal	rate
Monte Carlo statistics	$\pm 2\%$	signal	rate
selection efficiency	$\pm 5\%$ per jet	signal	rate
PDFs	$^{+3.5}_{-4.5}\%$	signal	rate
jet energy scale	$\pm 4.5\%$	signal	rate/shape
b/c M_{VTX}	3%	signal/backgrounds	shape
mistag M_{VTX}	3%	backgrounds	shape
bbC vs bbQ	uniform mix	backgrounds	shape
bbB vs bBb	uniform mix	backgrounds	shape
mistag asymmetry factor λ	1.4 ± 0.2	backgrounds	rate/shape
heavy flavor fractions	$\pm 50\%$	backgrounds	rate

IV. SYSTEMATIC UNCERTAINTIES

Several sources of systematic uncertainty on the signal and background contributions are considered. These can take the form of uncertainties on the rate of signal and background events which will be generated in pseudoexperiments, or on the shapes of the templates used to sample the event properties in the pseudoexperiments. A summary is shown in Table I. Shape uncertainties are introduced by modifying the templates used when throwing pseudoexperiments using an interpolation procedure, then fitting that modified pseudodata using the original default templates.

Rate uncertainties on the signal contribution relate to the number of events expected for a given cross section. They include the integrated luminosity of the data sample, the statistical errors due to the finite size of the generated signal samples, the efficiency of the trigger and SECVTX tagging requirements, and the effect on the efficiency due to uncertainties on PDFs.

Shape uncertainties are applied to the corrections used for jet energy scale and SECVTX tag mass modeling to match the data. Of these, the jet energy scale is the most significant source of uncertainty, particularly for Higgs masses below 120 GeV/c^2. As can be seen by comparing Figures 7 and 8, there is not a lot of difference between the m_{12} distributions for a low-mass Higgs and the background templates. The signal templates are more sharply peaked, however if the jet energy scale variation in a particular pseudoexperiment is large enough to move the peak in the pseudodata far from the peak in the default fit template, the fit is likely to ascribe many of the signal events in the pseudodata to one of the background templates instead of the signal, reducing the sensitivity. For higher Higgs masses the templates are less sharply peaked and not so similar to the background templates, so the loss in sensitivity is much less severe there.

The SECVTX tag mass M_{VTX} uncertainties are related to the parametrizations used to weight the events for the third jet tag bias, which are functions of m_{tag}. The bbq and bbc templates are too similar for the fit to constrain them both, so we use an average of the two as our default and interpolate between them to estimate a systematic uncertainty. In contrast, though we include both bbB and bBb templates in the fit, we must assume some relative ratio of the two when throwing pseudoexperiments. We conservatively assume a uniformly-distributed fraction of bbB between 0 and 100% of the total bbb component, with bBB constituting the remainder. Varying the value of λ used to subtract the non-$b\bar{b}$ component from the double-tagged events changes the shapes of the resulting corrected background templates but is found not to have a large effect.

Although we do not constrain any of the background components in the fits but rather allow them to float freely, we still must assume some normalizations in order to generate pseudoexperiments. For this purpose we use the PYTHIA generator-level samples discussed earlier. We find that in events with three or more jets, with at least two of them coming from $b/\bar{b}$ quarks, around 4% of the additional jets are from a c quark and 2% from another b quark in the event. Our background estimates from the double-tagged samples, after subtracting the non-$b\bar{b}$ contribution, are normalized to $N_{bbj}\epsilon_f$ where N_{bbj} is the number of three-jet events with two b-tagged jets and ϵ_f is the tag efficiency of the untagged jet if it were flavor f. Therefore, all that is needed to turn this into a rate prediction for triple-tagged events is to scale it by the fraction of jets which we believe to be flavor f. We assign an uncertainty of 50% to these flavor fractions and do not use these estimates as fit constraints, merely as a baseline from which to throw pseudoexperiments. For the bbQ and bQb templates use a normalization derived from the observed numbers of events with two b-tags (after subtraction) and a negative SECVTX tag in the additional jet, scaled by the asymmetry factor λ. This removes the reliance on simulation of the light-flavor mistag rate absolute normalization, which we do not believe is as well-modeled as that for heavy-flavor jets.

V. RESULTS

We begin with some simple fits of the data to show how the backgound templates work together. We also perform a fit with a signal template included for illustration. We move on to cross section times branching ratio limits for $bH, H \to b\bar{b}$ production in the case of a narrow standard model-like Higgs. Finally, we interpret our results as limits on $\tan\beta$ in the MSSM as a function of the pseudoscalar Higgs mass m_A, including the effects of the Higgs width.

A. Simple fits of the data

Figure 10 shows the result of a fit of the 9306 triple-tagged events observed in the data using the background templates only and with no systematic errors on the templates. We use a binned maximum-likelihood fit of two-dimensional templates in

FIG. 10: Fit of the triple-tagged data sample using only the QCD background templates, in the m_{12} and x_{tags} projections.

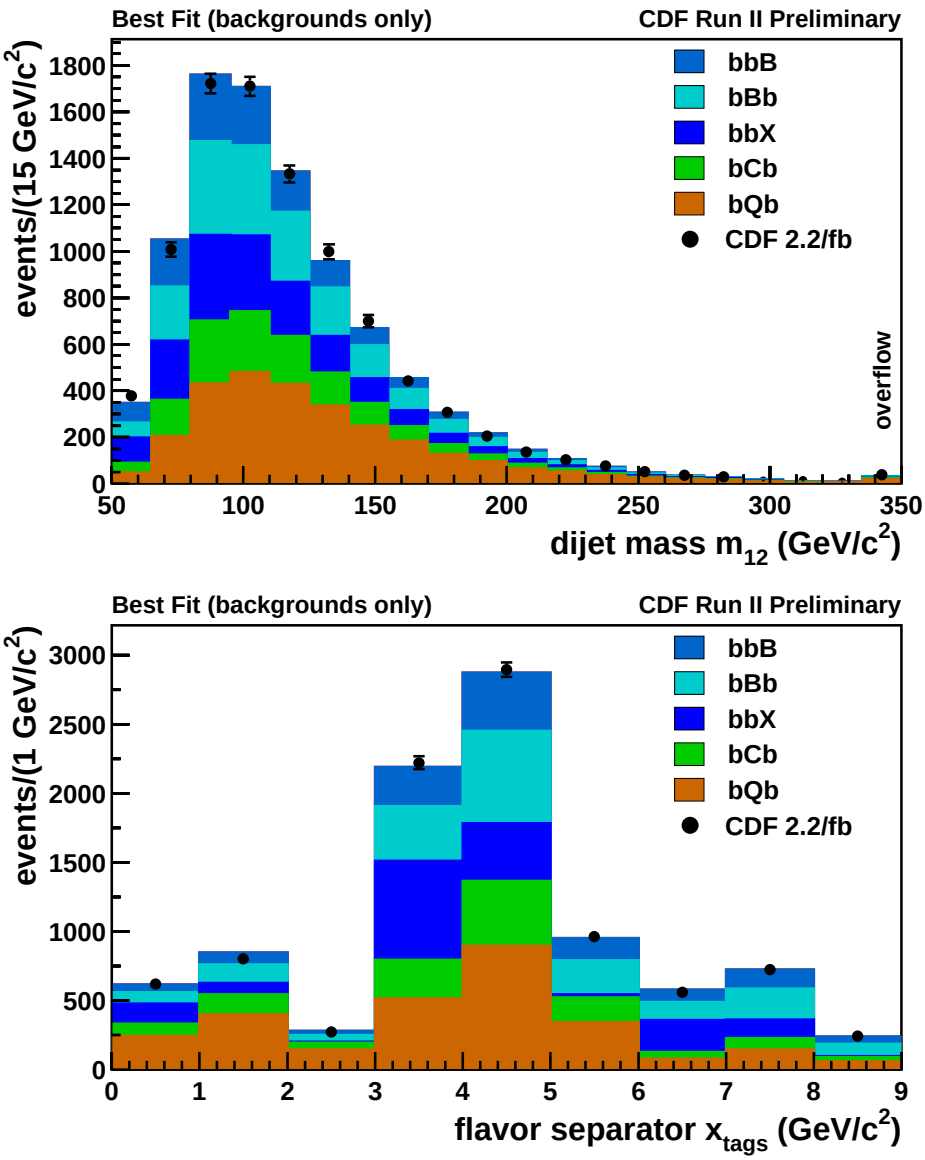

m_{12} versus x_{tags}; only the projections onto each axis are shown in Figure 10 are shown for clarity. The bbX component is the average of bbQ and bbC as discussed in the previous section. The χ^2/dof between the observed data and predicted background is 1.12. The numbers of fitted events for each background type are given in Table II. Also shown are the predicted numbers using the procedure described in the previous section that are the basis for pseudoexperiment generation.

A sample fit including a template for a Higgs mass of 150 GeV/c^2 is shown in Figure 11. In this case the χ^2/dof is 1.06, with the fit assigning 320±110 events

TABLE II: Numbers of fitted events for each background type, compared to the predictions derived from the PYTHIA heavy flavor fractions.

component	predicted	N_{fit}
bbB	1050	1320±490
bBb	2380	2010±500
bbX	1610	1770±140
bCb	1120	1370±560
bQb	2800	2840±350

TABLE III: Numbers of fitted events for each background type, compared to the predictions derived from the PYTHIA heavy flavor fractions.

component	N_{fit}
bbB	1900±550
bBb	1140±600
bbX	1720±140
bCb	1660±570
bQb	2570±360
Higgs	320±120

to the Higgs signal template. The numbers of fitted events for each component are shown in Table III.

B. Cross section times branching ratio limits

The limit calculations are performed using a custom program based on the MCLIMIT package [22]. It performs the fitting to either the observed distribution or to pseudoexperiments, and calculates confidence levels using the CL_s method.

Pseudoexperiments are generated using the results of the background-only fit in Figure 10. The background fractions and errors are used to determine how many of each type of event to generate in each pseudoexperiment. The nuisance parameters are set up to reproduce the anticorrelations as closely as possible, so that the total expected number of events in each pseudoexperiment is the same within 20-30 events. For pseudoexperiments that include Higgs signal, the expected signal fraction is subtracted from the background fractions in order to keep the average number of events constant.

Pseudoexperiments are generated based on the background predictions in Table II. For bbB and bBb we predict only the sum, and then use a uniform mix of the two with a flat distribution between the two extremes as discussed earlier. In this way we avoid any assumption about the relative weight of $b\bar{b}$ production through

FIG. 11: Fit of the triple-tagged data sample using the QCD background templates and one for $m_H = 150$ GeV/c^2.

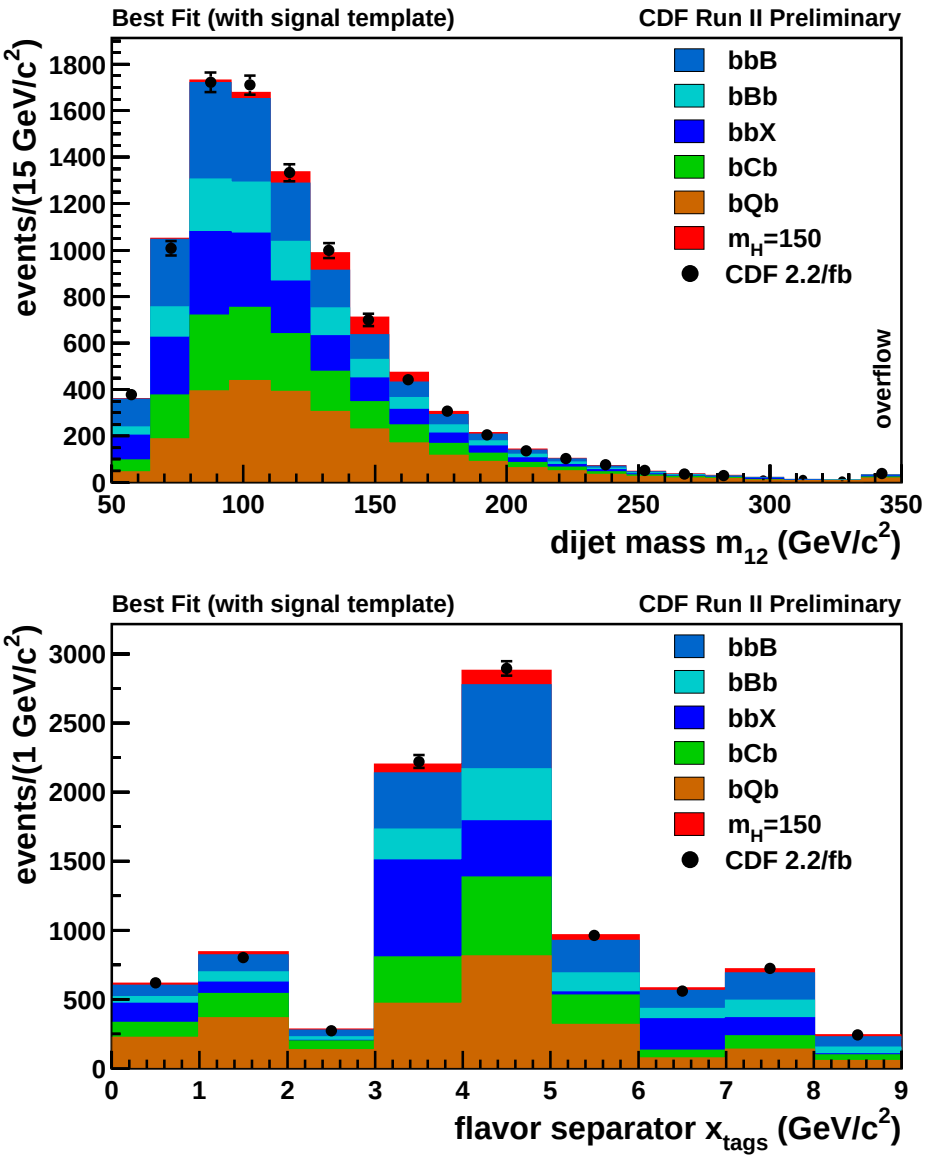

gluon splitting versus direct production. The number of signal events to generate depends on the assumed $\sigma \times BR$, the integrated luminosity, and the acceptance shown in Figure 6.

The median expected limits on $\sigma \times BR$ for statistics only with no systematic errors and with the full systematics including variations on the signal level and shape are shown in Table IV, along with the observed limits. The systematic errors increase the limits by 15-25% relative to the statistics-only case.

TABLE IV: Median expected and observed limits on $\sigma(p\bar{p} \to bH) \times BR(H \to b\bar{b})$, in pb.

m_H	no systematics	full systematics	observed
90	41.3	53.0	29.8
100	40.8	57.7	52.7
110	22.8	29.3	40.5
120	20.3	24.7	52.5
130	12.9	15.7	35.0
140	11.9	14.5	37.5
150	8.6	10.5	26.4
160	7.9	9.2	20.3
170	6.0	7.0	12.6
180	5.6	6.7	9.3
190	4.8	5.7	6.1
200	4.5	5.3	5.3
210	3.9	4.5	4.3

The expected and observed limits for the full systematics case are plotted as a function of the Higgs mass in Figure 12. Also shown are the bands resulting from calculating the expected limits using the $\pm 1\sigma$ and $\pm 2\sigma$ values of the test statistic from background-only pseudoexperiments. We observe a positive deviation of greater than 2σ from the expectation in the mass region of 130-160 GeV/c^2. The most significant discrepancy is at $m_H = 140$ GeV/c^2, with a 1-CL_b p-value of 0.9%. Including the trials factor, we expect to see a deviation of this magnitude at any mass in the range which we test (90-210 GeV/c^2 in steps of 10 GeV/c^2) in 5.7% of pseudoexperiments.

C. MSSM interpretation

These limits can be trivially converted into limits on $\tan\beta$ versus the pseudoscalar mass m_A in MSSM models by dividing by the standard model cross section times branching ratio (90%) (including the factor of two for h/H degeneracy) and taking the square root. The results of this are shown in Figure 13. The limits are not very realistic, however, because they do not include the effects of loop corrections which can enhance the cross section by more or less than $\tan^2\beta$ depending upon the MSSM scenario. They also do not include the effects of the Higgs width which can become significant when the down-type couplings are enhanced by such large factors.

Scaling the SM cross section by $2\tan^2\beta$ is correct at tree level, however loop effects can modify this relationship and introduce dependence on other parameters of the MSSM. In Ref. [1] an approximate expression for the cross section times branching ratio is given as:

FIG. 12: Median, 1σ, and 2σ expected limits, and observed limits versus m_H on linear (top) and logarithmic (bottom) scales.

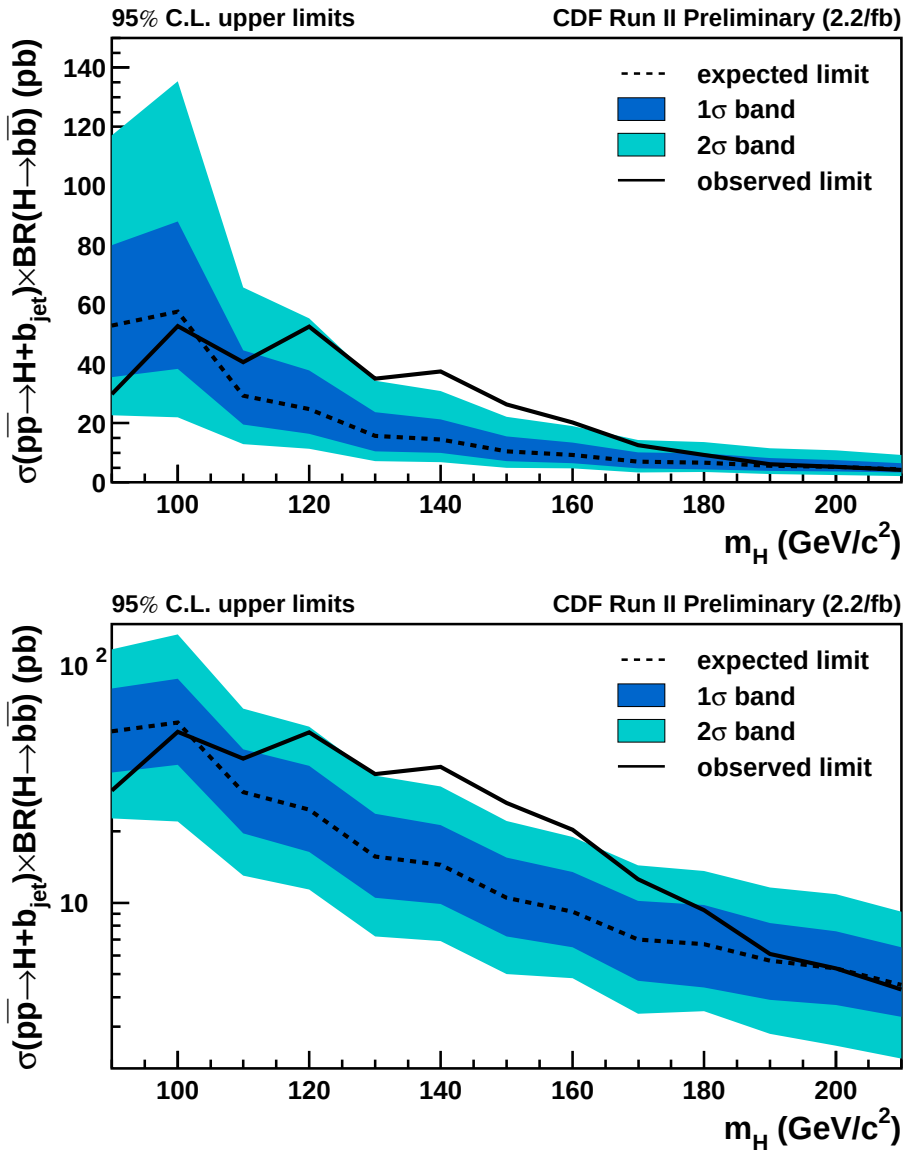

$$\sigma(b\bar{b}\phi) \times BR(A \to b\bar{b}) \simeq 2\sigma(b\bar{b}\phi)_{SM} \frac{\tan^2\beta}{(1+\Delta_b)^2} \times \frac{9}{(1+\Delta_b)^2+9} \tag{3}$$

where ϕ is a Higgs boson (either the SM variety or one of $h/H/A$), $\sigma(b\bar{b}\phi)_{SM}$ is the SM cross section, the factor of two comes from the degeneracy of A with either h or H, and the loop effects are incorporated into the Δ_b parameter. For our purposes it is important only to note that Δ_b is proportional to the product of $\tan\beta$ and the Higgsino mass parameter μ. Sample values of Δ_b given in Ref. [1] are -0.21

FIG. 13: Median, 1σ, and 2σ expected $\tan\beta$ limits (not including Higgs width effect or loop corrections), and the observed limits versus m_A.

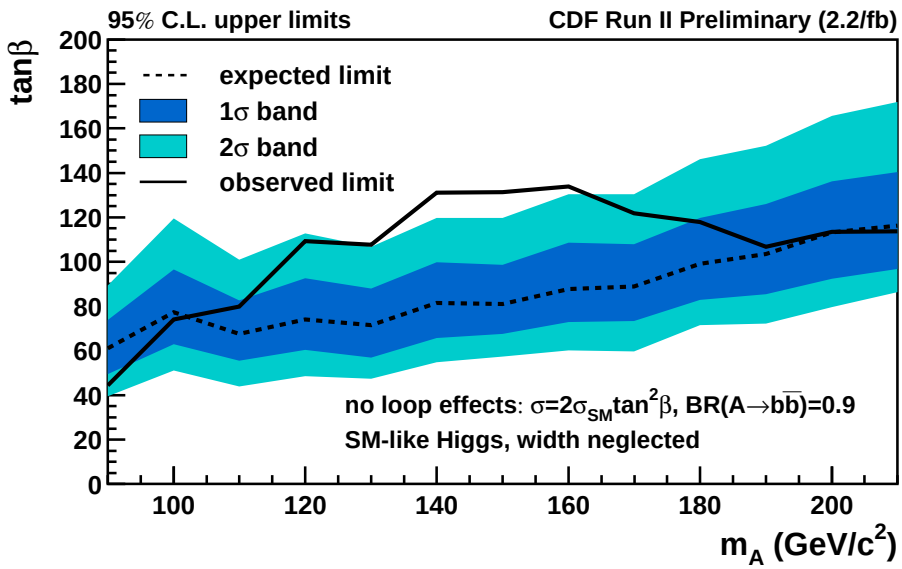

for the m_h^{max} scenario and -0.1 for the no-mixing scenario (at $\mu = -200$ GeV and $\tan\beta = 50$). It is apparent that negative values of μ and hence of Δ_b will increase the MSSM Higgs yield at fixed $\tan\beta$ above the tree level values and result in stronger limits on $\tan\beta$, while scenarios with μ positive will produce the opposite effect. Using Eqn. 3 we can predict the Higgs yield for any value of $\tan\beta$ and Δ_b and therefore derive limits in any desired scenario.

The limits shown in Figures 12 and 13 apply only to narrow Higgs like those in the standard model. If the cross section is increased by scaling the $b\bar{b}H$ coupling, as happens in the MSSM, then the width of the Higgs will increase as well. In order to account for this we convolute the cross section shown in Figure 5 with a relativisitic Breit-Wigner to produce cross section lineshapes for various values of the Higgs pole mass, $\tan\beta$, and Δ_b. Parametrizations of the partial widths $\Gamma_{b\bar{b}}$ and $\Gamma_{\tau\tau}$ as functions of m_A and $\tan\beta$ are obtained from the FEYNHIGGS [23] program, with $\Gamma_{b\bar{b}}$ also dependent on Δ_b.

Changing the width of the Higgs also changes the total cross section as a function of the pole mass. We integrate the broadened cross section described above for $m_H > 50$ GeV/c^2 (where the acceptance drops to zero) and divide by the no-width SM value to derive a correction factor. This factor ranges from 1.0-0.8 for pole mass of 90 GeV/c^2 to 1.0-1.1 for 180 GeV/c^2, for $\tan\beta$ from 40-120. The factor drops below 1 for low pole mass because part of the broadened cross section falls below the cutoff at 50 GeV/c^2. This information is needed when computing the expected number of events for a given Higgs mass and $\tan\beta$ value in the limits calculator.

FIG. 14: Distributions of m_{12} for varying $\tan\beta$ and $\Delta_b = 0$, for Higgs pole mass of 150 GeV/c^2. The normalizations indicate the acceptance relative to the SM case which has unit area.

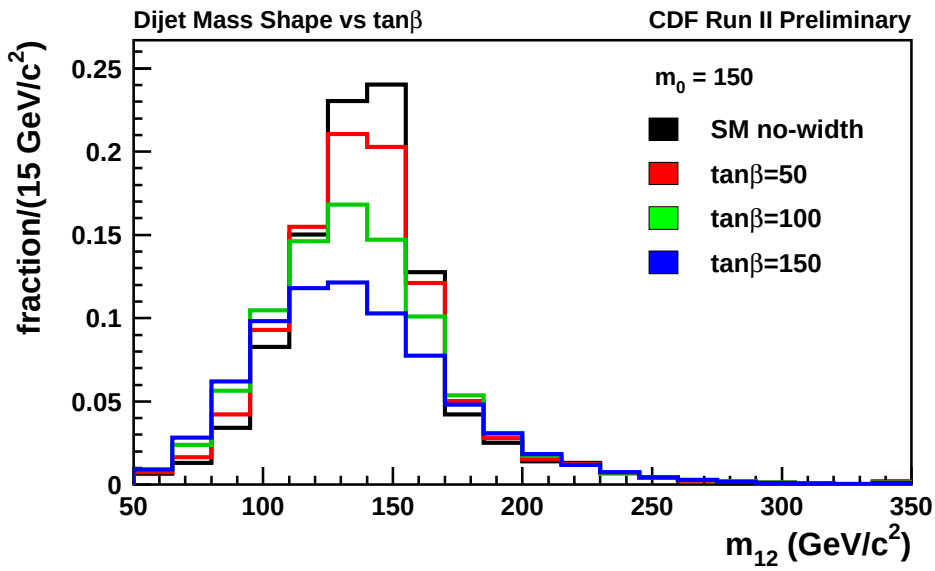

Fit templates as a function of $\tan\beta$ are constructed by combining the narrow-width templates, weighted by the m_H lineshapes and by the acceptance parametrization shown in Figure 6. An example is shown in Figure 14.

We scan in $\tan\beta$ in steps of 5 and calculate CL_s at each point, and exclude regions with $CL_s > 0.05$. The limits obtained are shown in Figure 15 for $\Delta_b = 0$. The limits get weaker in a highly $\tan\beta$-dependent way, so that compared with Figure 13 the -2σ contour moves much less than the $+2\sigma$ one does. This is because as $\tan\beta$ increases, the growing width spreads the events out over a larger region of m_{12}, reducing the fit power, and also tends to reduce the number of expected events due to the cross section lineshape extending downwards into regions with low or no acceptance.

Along with the $\Delta_b = 0$ case, limits are also generated for the m_h^{max} scenario with $\mu = -200$ GeV and are shown in Figure 16. Because of the relatively large and negative values of Δ_b in this scenario, the $\tan\beta$ limits are much stronger because we expect many more signal events for a given $\tan\beta$ relative to the $\Delta_b = 0$ case.

VI. CONCLUSION

A search for Higgs bosons produced in association with b-quarks is performed in 2.2 fb^{-1} of data. This process could be visible in supersymmetric models with high values of $\tan\beta$. The variable used is the mass of the two leading jets in triple-

FIG. 15: Median, 1σ, and 2σ expected limits, and the observed limits versus m_A, including the Higgs width and for $\Delta_b = 0$.

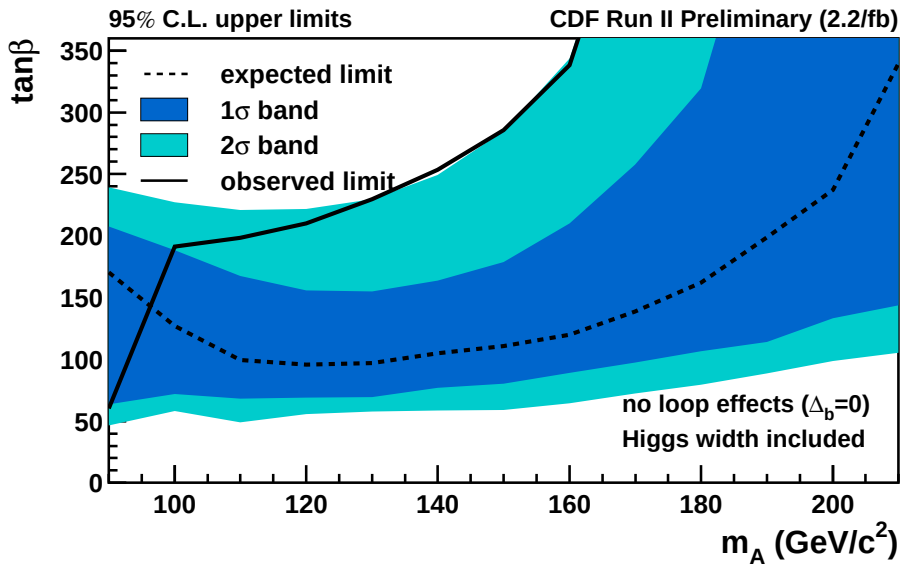

FIG. 16: Median, 1σ, and 2σ expected limits, and the observed limits versus m_H, including the Higgs width, for the m_h^{max} scenario with $\mu = -200$ GeV.

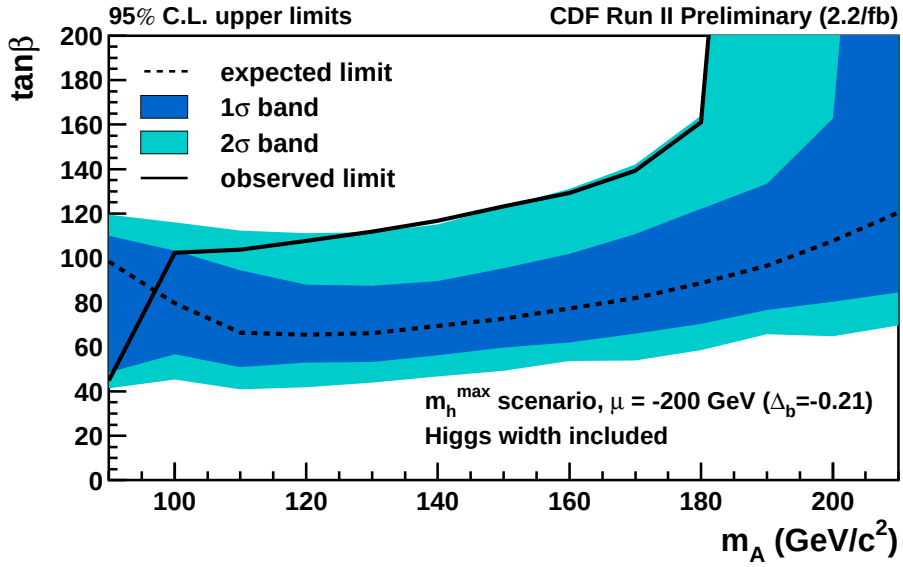

tagged events, with additional information from the SECVTX tag masses included to improve the background modeling.

We find an excess at about 140 GeV/c^2 in the narrow-width case, with a p-value of 0.9%. We estimate the probablility to observe such an excess at any mass at 5.7%. Otherwise the limits are within 2σ of expectations. It should be noted that the results in the narrow width case are applicable to other models of scalars decaying to $b\bar{b}$ produced in association with b quarks, they are not specific to standard model-like Higgs.

The results are also interpreted in two MSSM scenarios. In the case where loop effects are small, we find that the growth of the Higgs width as the couplings are enhanced permits only weak limits on $\tan\beta$. In the m_h^{max} scenario with μ negative, the enhanced production through loop effects allows exclusion of $\tan\beta$ values greater than 45 for $m_A = 90$ GeV/c^2 and about 105-140 for the mass range 110-170 GeV/c^2.

Acknowledgments

We thank the Fermilab staff and the technical staffs of the participating institutions for their vital contributions. This work was supported by the U.S. Department of Energy and National Science Foundation; the Italian Istituto Nazionale di Fisica Nucleare; the Ministry of Education, Culture, Sports, Science and Technology of Japan; the Natural Sciences and Engineering Research Council of Canada; the National Science Council of the Republic of China; the Swiss National Science Foundation; the A.P. Sloan Foundation; the Bundesministerium für Bildung und Forschung, Germany; the World Class University Program, the National Research Foundation of Korea; the Science and Technology Facilities Council and the Royal Society, UK; the Institut National de Physique Nucleaire et Physique des Particules/CNRS; the Russian Foundation for Basic Research; the Ministerio de Ciencia e Innovación, and Programa Consolider-Ingenio 2010, Spain; the Slovak R&D Agency; and the Academy of Finland.

---

[1] M. Carena, S. Heinemeyer, C. E. M. Wagner, and G. Weiglein, "MSSM Higgs boson searches at the Tevatron and the LHC: Impact of different benchmark scenarios," *Eur. Phys. J.* **C45** (2006) 797–814, `hep-ph/0511023`.

[2] F. Maltoni. `http://maltoni.home.cern.ch/maltoni/TeV4LHC/`.

[3] R. V. Harlander and W. B. Kilgore, "Higgs boson production in bottom quark fusion at next-to- next-to-leading order," *Phys. Rev.* **D68** (2003) 013001, `hep-ph/0304035`.

[4] S. Dawson, C. B. Jackson, L. Reina, and D. Wackeroth, "Higgs production in association with bottom quarks at hadron colliders," `hep-ph/0508293`.

[5] S. Dawson, C. B. Jackson, L. Reina, and D. Wackeroth, "Hadronic Higgs production with heavy quarks at the Tevatron and the LHC," `hep-ph/0603112`.

[6] J. Campbell, R. K. Ellis, F. Maltoni, and S. Willenbrock, "Higgs boson production in association with a single bottom quark," *Phys. Rev.* **D67** (2003) 095002,

hep-ph/0204093.

[7] J. Campbell *et al.*, "Higgs boson production in association with bottom quarks," hep-ph/0405302.

[8] **DØ** Collaboration, V. M. Abazov *et al.*, "Search for neutral supersymmetric Higgs bosons in multijet events at $\sqrt{s} = 1.96$ TeV," *Phys. Rev. Lett.* **95** (2005) 151801, hep-ex/0504018.

[9] **DØ** Collaboration, V. M. Abazov *et al.*, "Search for Neutral Higgs bosons in Multi-b-jet events in $p\bar{p}$ Collisions at $\sqrt{s} = 1.96$ TeV," *Phys. Rev. Lett.* **101** (2008) 221802, arXiv:0805.3556.

[10] **DØ** Collaboration, "Search for Neutral Higgs Bosons in Multi-b-jet Events," DONote 5726-CONF.

[11] **CDF** Collaboration, A. Abulencia *et al.*, "Search for neutral MSSM Higgs bosons decaying to tau pairs in $p\bar{p}$ collisions at $\sqrt{s} = 1.96$ TeV," *Phys. Rev. Lett.* **96** (2006) 011802, hep-ex/0508051.

[12] **CDF** Collaboration, "Search for Neutral MSSM Higgs Boson(s) Decaying to Tau Pairs with 1.8/fb of Data," CDF Note 9071.

[13] **DØ** Collaboration, V. M. Abazov *et al.*, "Search for neutral Higgs bosons decaying to τ pairs in $p\bar{p}$ collisions at $\sqrt{s} = 1.96$ TeV," *Phys. Rev. Lett.* **97** (2006) 121802, hep-ex/0605009.

[14] **DØ** Collaboration, V. M. Abazov *et al.*, "Search for Neutral Higgs Bosons at high $\tan\beta$ in the $b(h/H/A) \to b\tau\tau$ Channel," *Phys. Rev. Lett.* **102** (2009) 051804, arXiv:0811.0024.

[15] **DØ** Collaboration, "Search for MSSM Higgs boson production in di-tau final states with 2.2 fb^{-1} at the D0 detector," DONote 5740-CONF.

[16] **CDF** Collaboration, "Measurement of the $t\bar{t}$ production cross section in $p\bar{p}$ collisions at $\sqrt{s} = 1.96$ TeV using Lepton+Jets Events with Secondary Vertex b-Tagging," CDF Note 8795.

[17] **CDF** Collaboration, D. Acosta *et al.*, "Measurement of the J/ψ meson and $b-$hadron production cross sections in $p\bar{p}$ collisions at $\sqrt{s} = 1960$ GeV," *Phys. Rev.* **D71** (2005) 032001, hep-ex/0412071.

[18] W. K. Tung *et al.*, "Heavy quark mass effects in deep inelastic scattering and global QCD analysis," *JHEP* **02** (2007) 053, hep-ph/0611254.

[19] F. Maltoni, Z. Sullivan, and S. Willenbrock, "Higgs-boson production via bottom-quark fusion," *Phys. Rev.* **D67** (2003) 093005, hep-ph/0301033.

[20] T. Sjostrand, S. Mrenna, and P. Skands, "PYTHIA 6.4 physics and manual," *JHEP* **05** (2006) 026, hep-ph/0603175.

[21] **CDF** Collaboration, D. Acosta *et al.*, "Measurements of $b\bar{b}$ azimuthal production correlations in $p\bar{p}$ collisions at $\sqrt{s} = 1.8$ TeV," *Phys. Rev.* **D71** (2005) 092001, hep-ex/0412006.

[22] T. Junk and J. Heinrich. https://plone4.fnal.gov:4430/P0/phystat/packages/0711001.

[23] S. Heinemeyer *et al.* http://www.feynhiggs.de/.